would be Ce^{3+}- ($4f^1$) or Tb^{3+}- ($4f^8$) doped CaF_2 but not La^{3+}- or Lu^{3+}-doped samples, since La^{3+} ($4f^0$) has no $4f$ electron and Lu^{3+} ($4f^{14}$) has a $4f^{14} \rightarrow 14^{13}$ $5d$ transition even higher[15] than that of isolated Gd^{3+} ($4f^7$), i.e., far beyond the cutoff of CaF_2. We identify the sharp absorptions at 26 400 and 37 800 cm^{-1}, which occur only in the uv-switched photochromic samples[2,3] of 0.1%Ce : CaF_2 and 0.1% Tb : CaF_2, respectively, as the "red-shifted" transitions. They correspond to the transitions of $4f^1 \rightarrow 5d$ at 32 400 cm^{-1} for Ce^{3+} and $4f^8 \rightarrow 4f^7 5d$ at 46 600 cm^{-1} for Tb^{3+}, respectively, in ordinary[15] CaF_2. The amount of the down shift is 6000 cm^{-1} for Ce^{3+} ($4f^1$) and 8800 cm^{-1} for Tb^{3+} ($4f^8$). By interpolation we estimate that the lowest $4f^7 \rightarrow 4f^6 5d$ transition of Gd^{3+} in ordinary CaF_2 would be at 83 000 cm^{-1}, i.e., the sum of $4f^7 \rightarrow 4f^6 5d$ energy of Gd^{3+} in uv-switched CaF_2—74 500 cm^{-1}—and the interpolated down shift of 8400 cm^{-1} for Gd.

We have measured the ultraviolet spectra of nonphotochromic CaF_2 and have confirmed that the spectra presented in this paper are present only in the photochromic CaF_2 crystals.

In conclusion, our ultraviolet spectra of PC in CaF_2 is in general agreement with the present model[2,3,5,6] of vacancy-impurity complex.

ACKNOWLEDGMENTS

The author wishes to thank D. L. Staebler of RCA Laboratories for the generosity of supplying all samples, reprints, and comments; R. C. Alig of RCA for a preprint; B. Fitton and staff at ESTEC for hospitality and frequent assistance; A. Bishay at AUC for support and encouragement; and J. R. Henderson of McDonnell-Douglas Corp. for reading the manuscript.

*Present address: The American University in Cairo, Cairo, Egypt, U.A.R.

[1]Z. J. Kiss, Phys. Today 23, No. 1, 42 (1970).
[2]D. L. Staebler, Ph. D. thesis (Princeton University, 1970) (unpublished).
[3]D. L. Staebler and S. E. Schnatterly, Phys. Rev. B 3, 516 (1971).
[4]D. L. Staebler and Z. J. Kiss, Appl. Phys. Letters 14, 93 (1969).
[5]R. C. Alig, Phys. Rev. B 3, 536 (1971).
[6]C. H. Anderson and E. S. Sabisky, Phys. Rev. B 3, 527 (1971).
[7]E. Loh, Phys. Rev. 154, 270 (1967).
[8]E. Loh, Phys. Rev. 175, 533 (1968).
[9]F. Luty, in *Physics of Color Centers*, edited by W. B. Fowler (Academic, New York, 1968), p. 181.
[10]H. H. Tippins, Phys. Rev. B 1, 126 (1970).
[11]E. Loh, J. Chem. Phys. 44, 1940 (1966).
[12]Among the various rare-earth ions doped in CaF_2, the crystal-field strength on their $5d$ electron varies not more than a few hundred wave numbers [Refs. 7 and 13; E. Loh, Phys. Rev. 184, 348 (1969)]. Therefore, it is not possible from the present uv data to assign the local environment of the rare-earth ions involved in the charge transfer. The bandwidth of the charge transfer, however, may qualitatively indicate the uniformity of the local environment. For example, the bandwidth of 7500 cm^{-1} in Fig. 3 may involve more types of local environment of Ce^{3+} than that of La and Lu in Figs. 2 and 6, respectively, where the bandwidth is 5500 cm^{-1}.
[13]E. Loh, Phys. Rev. 158, 273 (1967).
[14]We also failed to switch this additively colored 0.1%Lu : CaF_2 to the ionized state at liquid-nitrogen temperatures (Refs. 2 and 3).
[15]E. Loh, Phys. Rev. 147, 332 (1966).

PHYSICAL REVIEW B VOLUME 4, NUMBER 6 15 SEPTEMBER 1971

LO-Phonon-Assisted Transitions in the Two-Photon Absorption Spectrum of KI†

Richard G. Stafford* and Kwangjai Park
Department of Physics, University of Oregon, Eugene, Oregon 97403
(Received 9 December 1970)

The two-photon absorption spectrum of KI is measured experimentally with high resolution in the exciton region at approximately 6 °K. Fine structure is resolved in which the $2P$ exciton is seen at 6.263 eV and a peak at 6.285 eV is identified as a LO-phonon-assisted transition. The exciton-phonon interaction is calculated using third-order time-dependent perturbation theory. The two-band model is used, where the two intermediate states are virtual excitons excited by the photons and the final state is composed of an exciton and LO-phonon. The theoretical prediction of the strength and location of the phonon-assisted peak agrees favorably with the experiment. Calculations are performed with several values for the hole mass; the value 3.0 is chosen as representing a good average for the fourfold-degenerate hole.

I. INTRODUCTION

Interest in the exciton-phonon interaction in alkali halides has been prevalent for some time. A considerable amount of work has been produced by Toyozawa on the general theory of the line shape

of exciton absorption spectra taking into account the effects of exciton-phonon coupling.[1-3] His primary results were that the exciton spectra become asymmetrically broadened and shifted in energy. The former effect has been established experimentally, where asymmetries are observed and half-widths have been measured.[4-6] The energy shifts have not been measured since they are much smaller than the relative shifts in the hydrogenic series caused by deviations in the electron-hole interactions from the normal Coulomb interaction. This latter effect is most pronounced in the $1S$ state which prevents it from being treated as a true Wannier exciton.

Recently, Baldini *et al.* have observed, via high-resolution reflectivity measurements, rather complex structure in the excitonic spectra of the alkali halides.[7] They found that exciton lines, instead of being only asymmetrically broadened, were resolved into numerous peaks; in particular, KI exhibited very anomalous behavior. The $1S$ exciton displayed a shoulder on the high-energy side separated by about 35 meV, whereas the $2S$ exciton was composed of four or five peaks spaced about 16.5 meV apart. Since the highest-energy phonon that can be linearly excited in KI has an energy of 18 meV, they attributed the former case to localized phonons created by quadratic terms in the exciton-phonon interaction and the latter to normal linearly excited phonons. The results presented on the reflectivity measurements were for a temperature of 6 °K. It is unfortunate that they did not fold the reflectivity spectra into the dielectric constant by a Kramers-Kronig inversion. This would have facilitated a clearer comparison of their results with previous one-photon absorption work and the present two-photon experiment.

A new method for studying the exciton-phonon interaction is provided by two-photon absorption spectroscopy. Two-quantum absorption was originally utilized by Hopfield *et al.* in studying the exciton regions of KI and CsI.[8,9] The two-photon technique offers very important advantages over the one-photon absorption method and the reflectivity approach. In one-photon absorption spectroscopy, one must work with very thin single crystals to study excitons, since the absorption constant in this region is typically around 10^5 cm^{-1}. However, it is very difficult to obtain samples that are free of strain in such a geometry. Another problem with thin crystals is the large surface-to-volume ratio, where owing to surface impurities and surface inhomogeneity, it becomes difficult to separate the surface-vs-bulk-volume effects. The latter problem is critical in reflectivity measurements regardless of the crystalline size, especially in resolving fine structure. This difficulty arises because the radiation penetration depth in regions of intrinsic absorption is only a few hundred angstroms.[10] In two-photon absorption, both light beams traverse the entire crystal. Since the crystal can be as large as physically possible, the surface-to-volume problem becomes negligible. Another serious difficulty with the one-photon method arises in comparing experiments with theory. Since the index of refraction varies rapidly in the exciton region, it must be made artificially smooth to allow the comparison using perturbation theory. However, in the two-photon work, both photons have individually $\hbar\omega \ll E_G - E_B$. This condition ensures that their respective indices of refraction are slowly varying and alleviates the comparison problem.

The experimental results of Hopfield *et al.* on KI exhibit weak structure in the $2P$ region of the absorption edge. Their theoretical approach did not allow for the degeneracy of the $P_{3/2}$ valence band and they pointed out that the $2P$ states are split into four levels according to the effective-mass theory for degenerate exciton bands. This degeneracy was attributed by them as the probable cause of the weak structure.

In view of the results of Baldini *et al.* and Hopfield *et al.*, and given the advantages of the two-phonon technique, it appeared desirable to us to perform a high-resolution two-photon absorption experiment on KI. The results of such an experiment are described in Sec. IV, and the experimental approach is described in Sec. II. The particular alkali halide KI was chosen not only because of the wealth of available experimental results on this material but in addition several advantages arise in isolating the exciton-phonon effects. Since E_B is much smaller than the spin-orbit splitting of the P valence band, the absorption spectrum is less complicated. Also, the S conduction band is fairly isolated from other conduction bands,[11] such as the D bands which cause very complicated spectra in other alkali halides.[12] An especially important feature is that $E_B \gg \hbar\omega_l$, which allows the exciton-phonon interaction to be tractable both experimentally and theoretically.

Exciton-phonon interactions have been considered previously in connection with a bound exciton-phonon state, the so-called exciton-phonon complex (EPC).[13,14] Toyozawa and Hermanson have formulated a theory to account for this effect,[15] treating the EPC as a quasiparticle. But their theory is valid only for $E_B \sim \hbar\omega_l$. In KI, $E_B \gg \hbar\omega_l$, so that their results are not applicable here.

A theoretical approach which accounts for the experimental results in Sec. IV is presented in Sec. III. However, a brief resume of previous work, along the lines followed in Sec. III, will be presented here to provide a basis for understanding the present approach.

The electron-phonon interaction has been studied extensively in the past. Fröhlich[16] first solved the

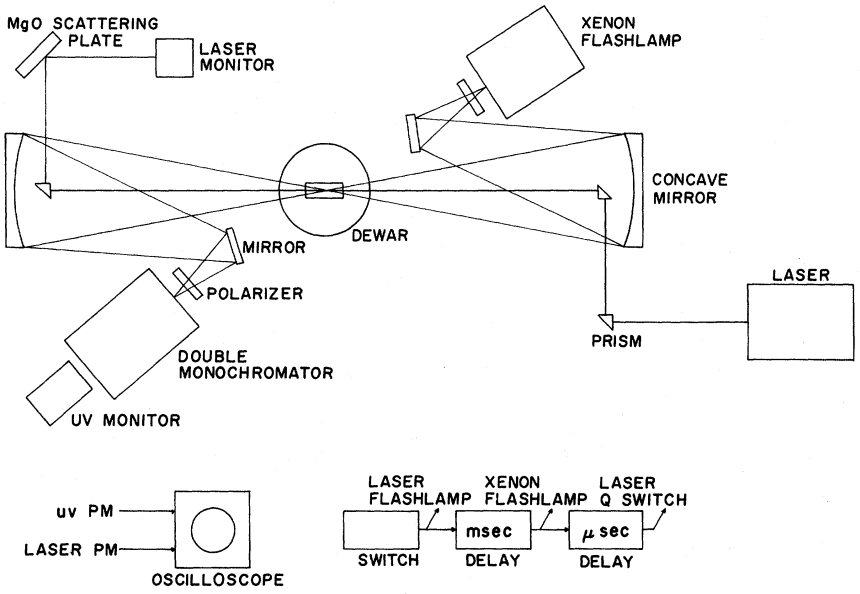

FIG. 1. Block diagram of the experimental apparatus.

dynamic problem of a Bloch electron moving through an ionic lattice and obtained the basic interaction Hamiltonian. His Hamiltonian treated LO phonons only, since they give rise to the largest electric fields. Ionic solids were chosen because the displacement of ions by phonons causes larger electric field than similar displacements in other solids. In the remainder of this paper, unless otherwise noted, phonons are taken as LO phonons exclusively.

Dumke[17] has applied a simplified version of the Fröhlich interaction to band-to-band transitions in semiconductors. He considered phonon-assisted optical absorption using second-order perturbation theory. In his approach, free electrons or holes (free in the sense of having negligible electron-hole attraction) could destroy a phonon near the Γ point. His solution was valid only at the band edge and in the absence of excitons. Thomas *et al.* extended the treatment to excitons,[18] also using an approximate interaction valid for the small exciton wave vector $\vec{K}$. Since the electron and hole are now bound, the pair acting as a quasiparticle absorb a phonon rather than either one having the phonon all to itself. This process again involves only phonon annihilation and was limited to the low-energy edge of an exciton resonance. Segall[19,20] and Mahan[20] extended the theory by including the exact Fröhlich interaction in the creation of an exciton by absorbing a photon and simultaneously scattering to $\vec{K}$ by destroying a phonon.

It should be noted that in the previous methods the case for phonon annihilation was considered only. The extension to include phonon creation was treated just recently.[21] The threshold for phonon annihilation is $E_{xn} - \hbar\omega_l$, whereas for creation it is $E_{xn} + \hbar\omega_l$.

II. EXPERIMENTAL METHODS

The experimental arrangement is quite similar to Hopfield and Worlock's earlier arrangement[9] and is shown in Fig. 1. Major improvements have been made to increase the resolution. The most important modifications will be mentioned first; a detailed description of the experiment will follow. The probe and laser beams are collinear and polarized, with their polarization vectors parallel. These features decreased the number of allowed final states, thereby making the comparison with theory simpler. A much longer sample, a more intense probe beam, and higher laser power are used to increase the signal-to-noise ratio. With a double monochromator, the scattered light was decreased. Concave aluminized mirrors were used instead of lenses to remove chromatic dispersion.

The essential elements of the experimental apparatus are shown in Fig. 1. The probe beam is from a pulsed xenon flashlamp (Xenon Corp., Suntron 4A) with a half-width of about 3 μsec. The beam is focused onto the sample and then refocused onto the entrance slit of the monochromator with one-to-one imaging using $f3.6$ optics. The concave mirrors are $f1.8$ with a 6 in. diam. A polarizer (Polacoat, uv) is mounted on the lamp housing, and another is placed in front of the monochromator to correct for the depolarization effects of the concave mirrors and sample.

The probe beam is scanned by a double monochromator consisting of two 0.25-m Eberts (Jarrell-Ash) in tandem. This geometry decreased the scattered light to less than one part in ten million. The monochromators were followed by a uv photomultiplier (RCA developmental type No. C70128)

which had negligible sensitivity, in the visible. Its useful range extended from approximately 2950–1050 Å. Since the phototube was exposed to the air, the higher-energy range above 2000 Å was not used. Because of the low-energy cutoff, no special filter was needed to exclude scattered laser light from the photomultiplier.

The laser beam was brought in collinear with the probe beam by means of several prisms. The beam was masked to 1-cm^2 cross section. After being attenuated, the unfocused beam has a peak intensity of 30 MW. The laser beam was attenuated, rather than using a weaker one, because of the nonlinear excitation properties of the ruby rod. The more intense the beam, the more homogeneous was its spatial intensity distribution. The monitoring of the laser occurred after the beam passed through the crystal. It was detected by a phototube (RCA 925). The MgO plate was used to ensure against nonlinear scattering with variations in the laser intensity.

The sample was a pure single crystal of KI (Harshaw Chemical Co.), 3 in. long with a surface 1 $\times\frac{1}{2}$ in. normal to the incident light. Since the crystal was cleaved to these dimensions and has O_h symmetry, orientation was simple to accomplish. The light was directed along the [100] axis and the polarization vectors were mutually parallel to [001]. Except for the two ends, the crystal was entirely enclosed in an aluminum jacket which was secured to the ceiling of the Dewar chamber. The temperature (6 °K) was monitored by a gallium-arsenide diode imbedded in the jacket.

When the sample was freshly cleaved, no laser damage was sustained if the beam did not touch the sides of the crystal and if no lens was used to focus the laser.

The procedure for triggering the various elements was as follows. A pushbutton triggers the laser flashlamp (~1-msec half-width). The triggering of the xenon flashlamp is delayed until the photon flux in the ruby rod is near a maximum. After firing the xenon (3-μsec half-width), the laser is Q switched (30-nsec half-width) when both flashlamp intensities are simultaneously at a maximum. The oscilloscope is triggered by the leading edge of the probe beam signal from the uv photomultiplier.

The pulses from the two phototubes were displayed simultaneously on a dual-beam oscilloscope (Tektronix, type 556). A representative photograph of the probe and laser intensities is displayed in Fig. 2. The oscilloscope sweep was running at 100 nsec/cm and a positive bias was added to the probe input so that only the absorption region was recorded on the screen. The upper trace is the laser-beam intensity and the lower is the probe beam, where the two-photon absorption effect is clearly discernible. Normally each photograph contained

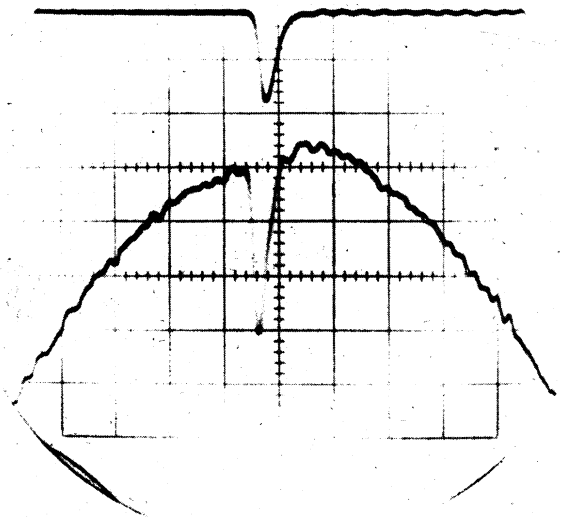

FIG. 2. Oscilloscope photograph of the probe and laser-beam signals showing the two-photon absorption effect.

five events with the probe beam intensity having much less curvature than shown in the figure. During the experiment, typically 30 events per spectral point were taken. To facilitate the data analysis, the oscilloscope photographs were enlarged by an opaque projector and the curves traced on graph paper. The major error was introduced in determining the incident intensity before absorption. The problem in estimating the original curve was compounded by shot noise riding on top of the probe signal.

The quantities which were then measured were the laser peak and the simultaneous signal dip and reconstructed incident probe intensity. Beer's law was applied to these intensities to yield the absorption constant. The resulting spectrum is a composite of several identical experiments, so that most points exhibit the results of around 100 events.

The accuracy of the data decomposes into two parts consisting of the absorption constant and the absorption constant per unit laser intensity. The former was limited chiefly by the shot noise from the probe-beam monitor, where the shot noise was typically 1% of the probe signal. In order to achieve this low level of shot noise, only six stages of the photomultiplier were used, while pushing it to the limit of its linearity. The upper limit of the photomultiplier linearity was experimentally determined, and the subsequent detection of the probe-beam intensity was done well below the saturation point of the photomultiplier (PM) tube by suitably attenuating the light output of the probe source. The PM electronics was very sensitive to transient sources of radiation, such as the laser Q switch. This source of noise was decreased to below the shot noise level by careful shielding of all signal carrying cables.

Noise with a time constant much smaller than the laser width was partially integrated by using 170-Ω coaxial cable between the PM and oscilloscope. The percentage absorption at 30 MW was about 10, so that the accuracy of the relative absorption constant was restricted by the shot noise to about 10%. The error in reading the oscilloscope screen gave a lower bound on this figure of around 2%.

Because the absorption constant depends linearly on the laser intensity for a given probe-beam wavelength, the normalized absorption constant is independent of laser intensity. Since this intensity has a large uncertainty, maybe a factor of 2 or higher, the normalization can have an error of greater than 50%. However, this is an error only in the scaling factor of the absorption constant, which does not affect the relative structure. The relative structure in the absorption constant can therefore be compared with the theory much more accurately than the absolute magnitude.

III. THEORETICAL METHODS

In this section we consider phonon-assisted two-photon absorption in insulators and apply the results to KI. With respect to perturbation theory, the subject divides into two parts: the determination of the two-photon matrix elements and separately the LO-phonon transition matrix elements. The theory of two-photon spectroscopy in solids has been treated before, the most successful work being Mahan's calculations of exciton transitions.[22] He uses a two-band model to construct Wannier excitons composed of electrons and holes from these bands. In the two-photon process, virtual excitons are included as intermediate states, and the final state is an exciton. The previous three-band models excluded the exciton intermediate states.[23] His results for the case where the conduction–to–valence-band dipole transition is allowed will be used extensively in the following calculations, since KI has a P valence band and a S conduction band.

For the phonon-assisted transitions, we adopt an approach similar to the previous treatments using phonon annihilation in optical-absorption spectra by Segall and Mahan.[19,20] The approach is modified, the difference being that we treat phonon creation, where a virtual exciton emits a phonon in reaching its final state. This method has already been applied to the phonon-assisted one-photon spectra,[21] and we now extend it to the two-photon case.

From third-order time-dependent perturbation theory, the probability of a vacuum-state exciton absorbing two photons (ω_1, ω_2) and simultaneously emitting a phonon (ω_l) in all possible sequences is given by

$$P_{fi}=\frac{2\pi}{\hbar}\left|\sum_{kl}\left(\frac{H^1_{fk}H^l_{kl}H^2_{li}}{(E_{1i}-\hbar\omega_2)(E_{ki}+\hbar\omega_l-\hbar\omega_2)}+\frac{H^2_{fk}H^l_{kl}H^1_{li}}{(E_{1i}-\hbar\omega_1)(E_{ki}+\hbar\omega_l-\hbar\omega_1)}+\frac{H^l_{fk}H^1_{kl}H^2_{li}}{(E_{1i}-\hbar\omega_2)(E_{ki}-\hbar\omega_1-\hbar\omega_2)}\right.\right.$$
$$\left.\left.+\frac{H^l_{fk}H^2_{kl}H^1_{li}}{(E_{1i}-\hbar\omega_1)(E_{ki}-\hbar\omega_2-\hbar\omega_1)}\right)\right|^2\delta(E_{fi}+\hbar\omega_l-\hbar\omega_1-\hbar\omega_2)\,. \qquad (1)$$

Presently, we are only interested in the two-photon energy region containing the bound-state excitons, i.e., E_G-E_B to E_G. For this case, if $\hbar\omega_1$, $\hbar\omega_2 \ll E_{ki}$, we have $\hbar\omega_1+\hbar\omega_2\approx E_{ki}$. Furthermore, if $\hbar\omega_1$, $\hbar\omega_2 \ll E_{1i}$, then the above expression, to good approximation, simplifies to

$$P_{fi}=\frac{2\pi}{\hbar}\left|\sum_k \frac{H^l_{fk}}{E_{ki}-\hbar\omega_1-\hbar\omega_2}\left[\sum_l\left(\frac{H^1_{kl}H^2_{li}}{(E_{1i}-\hbar\omega_2}+\frac{H^2_{kl}H^1_{li}}{(E_{1i}-\hbar\omega_1)}\right)\right]\right|^2$$
$$\times\delta(E_{fi}+\hbar\omega_l-\hbar\omega_1-\hbar\omega_2)\,. \qquad (2)$$

This three-quantum transtion is shown schematically in Fig. 3, where a vacuum-state exciton absorbs two photons in a vertical transition involving two intermediate states. The second virtual excitonic state then scatters into another excitonic state with wave vector $\vec{K}$ and simultaneously creates a phonon of wave vector $-\vec{K}$. Since KI has a P valence band and an S conduction band, the first intermediate state must be S exciton.[24] This limits the second intermediate state to P excitons. In the present experiment, with both photon polarization vectors parallel to $\hat{z}$, this last state must be P_z, i.e., $[n10]$, where $[nlm]$ represents a Wannier exciton with hydrogenic quantum numbers n, l, m.

In Eq. (2), the expression in square brackets is the two-photon transition matrix element which has been evaluated by Mahan in closed form.[22] Under the previous conditions, letting $\omega_1=\omega_L$ (fixed laser) and $\omega_2=\omega$ (variable probe), we have

$$\sum_l\left(\frac{H^2_{kl}H^1_{li}}{E_{1i}-\hbar\omega_1}+\frac{H^1_{kl}H^2_{li}}{E_{1i}-\hbar\omega_2}\right)$$
$$=\frac{(V)^{1/2}e^2}{\mu mc^2}\,A(\omega)A(\omega_L)\,\langle c|p_z|v\rangle$$
$$\times\frac{\hbar[(n^2-1)/n^5]^{1/2}}{[iE_B(3\pi a^5)^{1/2}]}\,[J_n(K)+J_n(K_L)]\,, \qquad (3)$$

where n is the principal quantum number of the kth $[n10]$ exciton, and

$$J_n(K)=\frac{\Gamma(1-K)K^2}{2t_0^{2+K}}\sum_{l=0}^{n-2}\frac{(2-n)_l}{l!}\left(\frac{K}{nt_0}\right)\left(\frac{\Gamma(1+2)}{\Gamma(1+3-K)}F(1-K,-K;1+3-K;1-t_0)\right.$$

$$\left.-\frac{K}{2nt_0}\frac{\Gamma(1+3)}{\Gamma(1+4-K)}F(1-K,-K;1+4-K;1-t_0)\right), \quad (4)$$

$$K^2=E_B/(E_G-\hbar\omega)\,,\quad t_0=\tfrac{1}{2}(1+K/n)\,.$$

The exciton-phonon matrix element is evaluated using the Fröhlich interaction Hamiltonian.[16] The resulting matrix element is

$$H_{fk}^{l}=u(q)\,\langle f|\,U(q)\,|k\rangle\,, \quad (5)$$

where

$$u(q)=i[e^2 2\pi\hbar\omega_l V^{-1}(\epsilon_\infty^{-1}-\epsilon_s^{-1})]^{1/2}q^{-1}\,,$$

$$\langle f|\,U(q)\,|k\rangle=\int d^3r\,\phi_f^*(r)(e^{i\vec{Q}_e\cdot\vec{r}}-e^{i\vec{Q}_h\cdot\vec{r}})\,\phi_k(r)\,,$$

and

$$Q_{e,h}=(M_{e,h}/M)q\,.$$

An important parameter in Eq. (3) is $\langle c|p_z|v\rangle$, which must be determined experimentally. In one-photon absorption, an exciton with a Lorentzian line shape has an absorption constant given by

$$\alpha_n(\hbar\omega)=\frac{8\pi e^2|\langle c|p_z|v\rangle|^2}{ncm^2(na)^3\omega}\,\frac{\Gamma_n/2\pi}{(\hbar\omega-E_{xn}^0)^2+\frac{1}{4}\Gamma_n^2}\,. \quad (6)$$

Therefore, letting $\alpha_{1s}(E_{x1})=\alpha_0$, we have

$$|\langle c|p_z|v\rangle|^2=ncm^2a^3E_{x1}\Gamma_{1s}\alpha_0/16e^2\hbar\,.$$

Now $A(\omega)=(c/n)(2\pi\hbar\rho/\omega)^{1/2}$ and $A(\omega_L)=(c/n_L)(2\pi\hbar\rho_L/\omega_L)^{1/2}$. Since ω and ω_L are in the transparent region of KI, we can let $n\approx n_L\approx\sqrt{\epsilon_\infty}$. Using $E_B=e^2/2\epsilon_\infty a$, the transition probability is

$$P_{n'}^{\vec{q}}(\hbar\omega)=\frac{4\pi^3(\epsilon_\infty^{-1}-\epsilon_s^{-1})nc(\hbar\omega_l)\hbar^2E_{x1}^0\rho\rho_L\Gamma_{1s}\alpha_0}{3\mu^2\omega\omega_L q^2}$$

$$\times\left|\sum_n\frac{\langle n'|\,U(q)\,|n\rangle}{E_{xn}^0-\hbar\omega_L-\hbar\omega}\left(\frac{n^2-1}{n^5}\right)^{1/2}[J_n(K)+J_n(K_L)]\right|^2$$

$$\times\delta(E_{xn}^q+\hbar\omega_l-\hbar\omega_L-\hbar\omega)\,, \quad (7)$$

where $E_{xn}^q=E_{xn}^0+\hbar^2q^2/2M$; $E_{xn'}^0=E_G-E_B/n'^2$ is the energy of an $[n'lm]$ exciton at the Γ point, and

$$\langle n'|\,U(q)\,|n\rangle\equiv\langle n'l'm'|\,U(q)\,|n10\rangle\,.$$

The contribution to the absorption constant of the probe beam caused by creating $[n'l'm']$ excitons is obtained by summing Eq. (7) over all final $\vec{q}$ states:

$$\alpha^{n'}(\hbar\omega)=\frac{2n}{Nc}\,\frac{V}{(2\pi)^3}\int d^3q\,P_{n'}^{\vec{q}}(\hbar\omega). \quad (8)$$

Integrating over the δ function, we find

$$\alpha^{n'}(\hbar\omega)=\xi(\hbar\omega)\Delta_{n'}^{-1/2}F^{n'}(\hbar\omega)\,, \quad (9)$$

where

$$\xi(\hbar\omega)=\frac{2\pi n^2(\epsilon_\infty^{-1}-\epsilon_s^{-1})(\hbar\omega_l)\hbar^3E_{x1}^0(2M)^{1/2}\rho_L\Gamma_{1s}\alpha_0}{3\mu^2(\hbar\omega_l)(\hbar\omega)}$$

$$F^{n'}(\hbar\omega)=\frac{1}{4\pi}\int d\Omega\left|\sum_n\frac{\langle n'|\,U(q)\,|n\rangle}{E_{xn}-\hbar\omega_L-\hbar\omega}\left(\frac{n^2-1}{n^5}\right)^{1/2}\right.$$

$$\left.\times[J_n(K)+J_n(K_L)]\right|^2,$$

$$\Delta_n=\hbar^2q^2/2M=\hbar\omega+\hbar\omega_L-\hbar\omega_l-E_{xn}^0\,.$$

The sum on n is over all $[n10]$ states. All final states $[n'l'm']$ are allowed for which energy conservation holds, since the LO-phonon interaction Hamiltonian contains all possible symmetries. The final states of interest to us are [100], [200], [210], and [21±1]. To illustrate the basic behavior of α for these states, the sum over the first two intermediate states is sufficient. This point has been treated in detail elsewhere.[21] Basically, what happens is that each succeeding term is much smaller than the preceding, so that the basic absorption structure is determined by the leading terms. However, due to the increase in density of states with

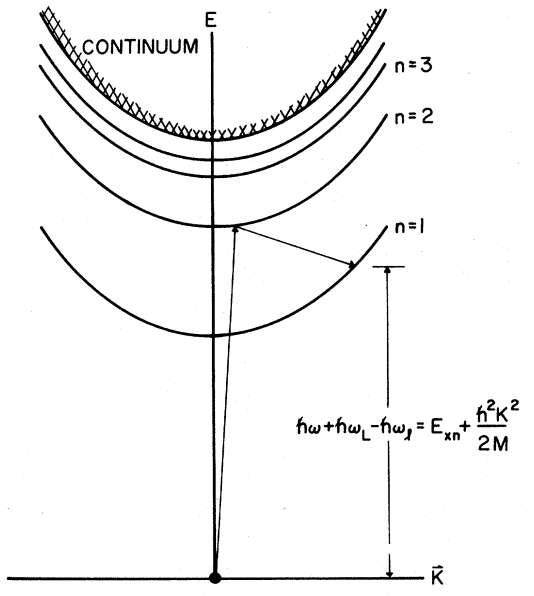

FIG. 3. Schematic of the simultaneous creation of an exciton and a phonon by an annihilation of two photons. The dot at $E=0$ is the crystalline ground state (excitonic vacuum state). The parabolas represent the hydrogenic exciton bands, going from the discrete to the continuum.

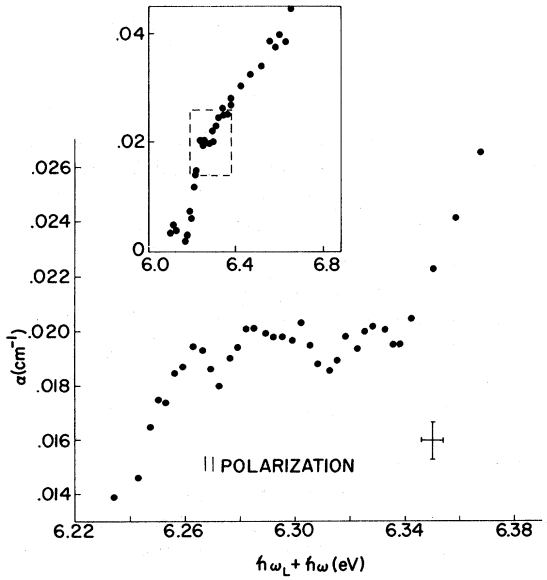

FIG. 4. Experimental two-photon absorption constant vs two-photon energy. The laser photon density is about 10^{15} photons/cm^3. The vertical error bar includes all of the acceptable experimental events for a given energy. Although there were not enough events per spectral point to do good statistics, a rough rms deviation would certainly be at most one-half of the indicated vertical bar. The boxed figure is extracted from K. Park and R. G. Stafford [Phys. Rev. Letters 22, 1426 (1969)].

energy, the neglected terms give an appreciable, but smooth background, so that the major contribution of these terms is to raise or lower the approximate expression for α.

IV. RESULTS

The experimental two-photon absorption constant in the exciton region is shown in Fig. 4. The boxed graph extends over a larger range, well into the band-to-band transitions and is a composite of previous experiments.[8,9,25] The spectrum clearly shows resolved structure that is sharper than expected from previous estimates of phonon broadening.[9,22] Taking Hopfield and Worlock's estimate of the band-gap and exciton binding energies ($E_G = 6.34$ eV, $E_B = 0.35$ eV),[9] there should be $2P$, $3P$, and $4P$ excitons at 6.253, 6.301, and 6.318 eV, respectively. The experimental peak at 6.263 eV can only be the $2P$ exciton at the Γ point since it is energetically the first allowed two-photon transition. The 0.01-eV discrepancy in peak location can probably be partially accounted for by the crystalline field splitting of the $2S$-$2P$ hydrogenic degeneracy. However, since E_G and E_B have been determined only indirectly,[9] the $2S$-$2P$ shift cannot be determined in the above fashion. Problems also are encountered in the experimental determination of the $2S$ peak. Results from emission spectra at[26] 10 °K indicate a $2S$ energy of 6.22 eV, a value lower than either of the above which partly may be caused by the shift to lower energy due to higher temperature. However, in contrast to this temperature shift, Fisher and Hilsch[27] in a one-photon absorption experiment at 14 °K measured the $2S$ state at 6.24 eV. Again, in a reflectivity experiment at 6 °K, Baldini *et al.* obtained for the $2S$ position a value of 6.28 eV.[7] The experimental situation is clearly in disarray. In any case, the 0.01-eV shift is much smaller than the $1S$ shift. Since the $1S$ state lies at 5.87 eV,[26] but from the band parameters assumed here[9] should be at 5.99 eV, the latter shift is 0.12 eV.

The two spikes at 6.302 and 6.318 eV were repeatable to within ± 0.001 eV. They lie so close to the $3P$ and $4P$ positions that we tentatively designate them as such. Nothing can be achieved by considering the relative strengths of succeeding exciton lines, since the exciton-phonon interaction contributes quite strongly to absorption at the resonances, as will shortly be shown. Beyond the $4P$ state, the spectrum rapidly approaches the rising straight line predicted by Mahan[22] and verified by Hopfield and Worlock.[9] These results appear to emphasize the validity of using Wannier excitons in insulators except for the anomalous $1S$ state.

The most interesting part of Fig. 4 is the relatively broad peak at 6.285 eV which lies in a position that cannot be accounted for in the simple two-photon formalism using Wannier excitons. However, if one invokes the phonon-assisted interaction of Sec. III, the situation becomes quite promising. Evaluating Eq. (9) by computer, we find the theoretical phonon-assisted contribution to the two-photon absorption constant, of which the logarithm is plotted in Fig. 5. The plot is a composite of the [100], [200], [210], and [21± 1] final exciton states. The first has a threshold at $E_{x1}^0 + \hbar\omega_l$, and the others at $E_{x2}^0 + \hbar\omega_l$. While the use of the effective-mass approximation is open to question for [100] in this energy range, it is certainly justified for the other states. The LO-phonon energy is[7] 0.018 eV and the value chosen for the hole mass is 3.0. The interesting structure near the $2S$ position is the result of quantum-mechanical interference in the phonon-assisted transition to the $1S$ final state. It is the virtual intermediate states which interfere with one another, and this effect has been treated in detail elsewhere.[21] In the δ-function approximation, the phonon-assisted transitions become singular at the exciton resonances. The spikes at $2S$ and $3S$ indicate this behavior, where [100] causes the peak at 6.253 eV, and [100], [200], [210], [21± 1] contribute to the peak at 6.301 eV. The phonon-assisted threshold for $n = 2$ states is shown by I. The peak at II is 6.275 eV and results chiefly from a linear superposition of the rapidly varying transitions to [200], [210], and [21± 1]. A linear plot of the latter

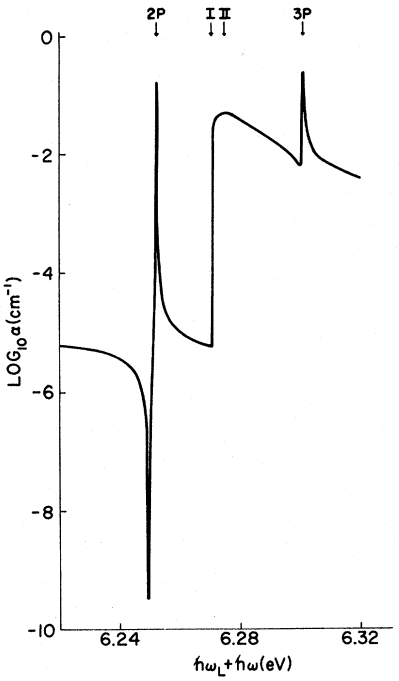

FIG. 5. Logarithm of the theoretical two-photon LO-phonon-assisted absorption constant vs two-photon energy. The hole mass is 3.0 and the laser photon density is about 10^{16} photons/cm^3.

structure is given in Fig. 6, which shows the narrowness of the phonon-assisted transition.

A few words should be said about the choice of the hole mass. There are no experimental measurements of M_h because of its large value.[11] Theoretical calculations have been performed by Onodera *et al.*, where they chose the band-gap energy to be 6.20 eV at 80 °K.[11,12] This value is actually the position of the absorption shoulder,[4] which is caused by excitons and is not the absorption band edge due to band-to-band transitions. Eby *et al.* incorrectly interpreted this shoulder as being associated with the onset of band-to-band transitions.[4] The shoulder has been solidly established as due to excitons; the shoulder turns into a flat region and this merges continuously with the band-to-band transitions.[24] More recent works give E_G as 6.31 eV at 10 °K,[6,26] and 6.34 eV at 4.2 °K.[9] For the effective electron mass, Onodera and Okazaki derive 0.49,[11] which is much larger than the experimental value of 0.398.[28]

The determination of M_h is complicated due to a degenerate $P_{3/2}$ valence band. This Γ_8^- valence band is fourfold degenerate, composed of two doubly degenerate bands. At $\vec{K}=0$, the states are a linear superposition of P orbitals with azimuthal quantum numbers $\pm\frac{3}{2}$ and $\pm\frac{1}{2}$ where the mixing is determined from $\vec{k}\cdot\vec{p}$ perturbation theory using the crystalline field. In this fashion, Kittel[29] obtains the following expression for the energy splitting of the hole band:

$$E(\vec{k}) = Ak^2 \pm [B^2k^4 + C^2(k_x^2k_y^2 + k_y^2k_z^2 + k_z^2k_x^2)]^{1/2} . \tag{10}$$

For these parameters, Onodera and Okazaki find $2mA/\hbar^2 = -0.4$, $2m|B|/\hbar^2 = 0.2$, and $2m|C|/\hbar^2 = 0.0$.[11] Since $E(\vec{k}) = \hbar^2k^2/2m_h^*$, this gives us two hole masses ($M_h = -1.67, -5.0$). These are much larger than the effective electron mass. No attempt has been made here to take into account degenerate band theory in our calculation, except in using a suitable average value for the hole mass. In Fig. 7, the absorption constant in the region of the phonon-assisted peak is plotted for several values of the hole mass, where the variation of M_h is over a reasonable range. It can be seen that the strength of the phonon-assisted transition is critically dependent on the ratio of the hole and electron masses. If $M_e = M_h$, then the effect would be zero since the exciton would then be effectively neutral. In an earlier letter,[30,31] we used a value for M_h of 1.0, which is smaller than the result of Onodera and Okazaki's calculations.

With a hole mass of 3.0, the separation of the $2P$ and phonon-assisted peaks is 22.5 meV, which is close to the experimental spacing of 22 meV. It can be seen that the theory reproduces the experimental situation very well.

The experimental parameters used in the calculations are given elsewhere,[21] with the exception of the hole mass and the laser intensity. A very rough estimate of the laser is 30 MW, which gives a pho-

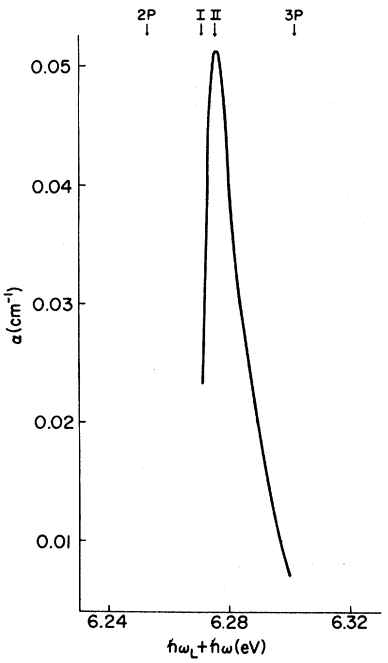

FIG. 6. Linear plot of Fig. 5. in the region about II.

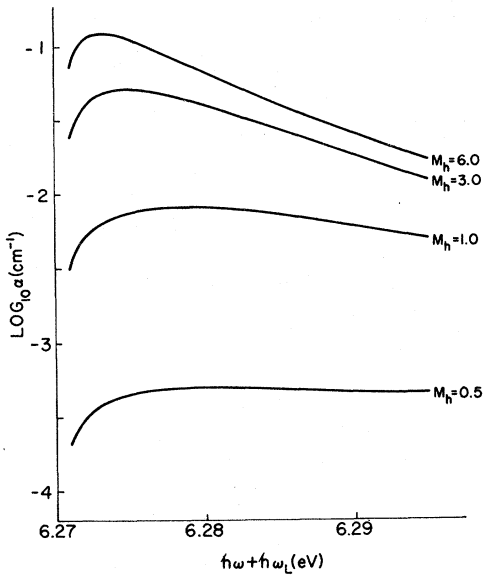

FIG. 7. Parametric dependence of the logarithm of the absorption constant on the electron-hole mass ratio in the region about II in Fig. 5.

ton density of approximately 10^{16} photons/cm^3. Since the absorption constant depends linearly on the laser photon density when I (probe)/I(laser) $\ll 1$, the laser acts merely as a scaling factor so that its rough determination is not crucial.

V. CONCLUSION

It has been shown that the two-photon absorption technique can be a powerful tool in the study of the fundamental interactions in solids. The experimental results agree so well with the theoretical calculations that it seems quite conclusive that the LO-phonon-assisted transitions play an important part in the absorption spectra of KI. With this initial impetus, several improvements in the experimental and theoretical methods immediately suggest themselves.

The present experiment was chiefly instrument resolution limited. Resolution can be improved by going to lower temperatures and using a monochromator with better dispersion characteristics and narrower slit widths. It would be desirable to increase the resolution to study the broadening effects of the acoustic phonons. It has been previously stated[22] that the $2P$ exciton state was not resolvable because of its closeness to other exciton lines and its large width. Since we have resolved this state, its width cannot be as large as supposed. A further indication of the possible weakness of the acoustic phonon interaction is the sharpness of the spikes at the $3P$ and $4P$ positions.

In conjunction with experimental improvements increasing the resolution, the theory should also be extended to include acoustic phonon broadening and degenerate $\vec{k}\cdot\vec{p}$ perturbation theory. The latter must include not only the splitting of the valence bands, but the degeneracy of the excitons as well. With these improvements, it might be possible to study the relative strengths of the exciton and phonon-assisted transitions.

Of further interest is the interference effect at the low-energy side of the $2S$ state. This effect has such a small absorption constant that the signal-to-noise ratio must be considerably improved to observe it. To pursue the effect more carefully, more intermediate states should be included in the numerical evaluation of Eq. (9) to provide an accurate background for the leading terms to interfere with. The previous work on phonon-assisted one-photon absorption showed the shifting of the interference minimum with the exact-vs-approximate spectra. More serious is the questionable existence of effective-mass states in this region. For this reason, it is important to measure the phonon-assisted transition from threshold at $E_{x1}^0 + \hbar\omega_l$ up to E_{x2}^0. The absorption in this range is around 10^{-5} cm^{-1}, so that detection will be difficult.

As mentioned, only the parallel-polarization spectrum of the two beams was studied. The perpendicular polarization was also measured, but the signal-to-noise ratio was not good enough to resolve any structure. For this case, the absorption constant was typically 60% of the parallel geometry. The polarization dependence of the probe and laser beams should be measured more completely so that the relations between states with different symmetries can be compared with the group-theoretical predictions.

Finally, it would be advantageous to extend the experiments to other solids to test the generality of the theory. In particular, one should choose a system with a well-established Wannier series, such as Cu_2O, since the present exciton-phonon interaction was calculated using Wannier excitons. Slight modifications would have to be incurred, however, since this insulator has a D valence band.[32,33] Some other interesting solids are RbI, MgO, ZnO, CdS, and PbI_2.

ACKNOWLEDGMENT

We would like to thank G. D. Mahan for his suggestions and many discussions.

†Research supported in part by the National Science Foundation.

*To be submitted in partial fulfillment of the requirements for the Ph. D. degree at the University of Oregon, Eugene, Ore. 97403.

[1]Y. Toyozawa, Progr. Theoret. Phys. (Kyoto) 20, 53

(1958).
[2]Y. Toyozawa, Progr. Theoret. Phys. (Kyoto) 27, 89 (1962).
[3]Y. Toyozawa, J. Phys. Chem. Solids 25, 59 (1964).
[4]J. E. Eby, K. J. Teegarden, and D. B. Dutton, Phys. Rev. 116, 1099 (1959).
[5]H. R. Philipp and H. Ehrenreich, Phys. Rev. 131, 2016 (1963).
[6]K. Teegarden and G. Baldini, Phys. Rev. 155, 896 (1967).
[7]G. Baldini, A. Bosacchi, and B. Bosacchi, Phys. Rev. Letters 23, 846 (1969).
[8]J. J. Hopfield, J. M. Worlock, and K. Park, Phys. Rev. Letters 11, 414 (1963).
[9]J. J. Hopfield and J. M. Worlock, Phys. Rev. 137, A1455 (1965).
[10]M. L. Cohen, P. J. Lin, D. M. Roessler, and W. C. Walker, Phys. Rev. 155, 992 (1967).
[11]Y. Onodera and M. Okazaki, J. Phys. Soc. Japan 21, 2229 (1966).
[12]Y. Onodera and Y. Toyozawa, J. Phys. Soc. Japan 22, 833 (1967).
[13]W. Y. Liang and A. D. Yoffe, Phys. Rev. Letters 20, 59 (1968).
[14]W. C. Walker, D. M. Roessler, and E. Loh, Phys. Rev. Letters 20, 847 (1968).
[15]Y. Toyozawa and J. Hermanson, Phys. Rev. Letters 21, 1637 (1968).
[16]H. Fröhlich, Advan. Phys. 3, 325 (1954).
[17]W. P. Dumke, Phys. Rev. 108, 1419 (1957).
[18]D. G. Thomas, J. J. Hopfield, and M. Power, Phys. Rev. 119, 570 (1960).
[19]B. Segall, Phys. Rev. 150, 734 (1966).
[20]B. Segall and G. D. Mahan, Phys. Rev. 171, 935 (1968).
[21]R. G. Stafford, Phys. Rev. B 3, 2729 (1971).
[22]G. D. Mahan, Phys. Rev. 170, 825 (1968).
[23]References cited in Ref. 22.
[24]R. J. Elliott, Phys. Rev. 108, 1384 (1957).
[25]K. Park and R. G. Stafford, Phys. Rev. Letters 22, 1426 (1969).
[26]J. Ramamurti and K. Teegarden, Phys. Rev. 145, 698 (1966).
[27]F. Fischer and R. Hilsch, Nachr. Akad. Wiss. Göttingen, II Math.-Physik. Kl. 8, 241 (1959).
[28]J. W. Hodby, J. A. Borders, and F. C. Brown, Phys. Rev. Letters 19, 952 (1967).
[29]C. Kittel, *Quantum Theory of Solids* (Wiley, New York, 1967).
[30]R. G. Stafford and K. Park, Phys. Rev. Letters 25, 1652 (1970).
[31]Note the absorption constant in Ref. 30 should be a factor of 4 smaller.
[32]R. J. Elliott, Phys. Rev. 124, 340 (1961).
[33]J. P. Dahl and A. C. Switendick, J. Phys. Chem. Solids 27, 931 (1966).

PHYSICAL REVIEW B VOLUME 4, NUMBER 6 15 SEPTEMBER 1971

Phonon Structure of Impurity-Related Optical Spectra in Insulators*

M. Mostoller, B. N. Ganguly, and R. F. Wood
Solid State Division, Oak Ridge National Laboratory, Oak Ridge, Tennessee 37830
(Received 14 January 1971)

The theory of optical processes associated with point imperfections in insulating crystals is briefly reviewed and a practical efficient computational procedure is developed for the detailed application of the theory to systems whose spectra exhibit marked vibronic structure. This procedure includes the following features: (a) an iterative scheme for extracting the effective one-phonon density of states from experimental data; (b) the convolution of the one-phonon spectrum to find the contributions of those n-phonon processes which yield discernible vibronic structure and the use of moment analysis for higher n-phonon processes; (c) inclusion of the lowest-order effects of quadratic coupling on the temperature dependence of the zero-phonon line's half-width and peak position; (d) a simple transformation between phonon operators in the ground and excited electronic states of the impurity which breaks the mirror symmetry between the absorption and emission spectra characteristic of the strict linear-coupling approximation. The absorption spectrum of the N_1 color center in NaCl, which exhibits a great deal of phonon structure, is used to illustrate certain aspects of the calculations. Good agreement between theory and experiment is obtained for this example.

I. INTRODUCTION

The modifications of the electronic and vibrational properties of crystals produced by the introduction of point imperfections[1] have been investigated extensively in recent years. A particularly large amount of work has been devoted to the study of the optical absorption and emission spectra of defects and impurities in insulators, which display great variety ranging from smooth broad bands with little or no vibronic structure to spectra in which only sharp structure is observed. Although the theory of these optical processes is well understood by now, the calculations involved in its detailed application can become quite complicated. In spite of this, it would seem that the great wealth of information about the interacting electron-phonon system which is inherent in the theory warrants